Physics Letters B 790 (2019) 498–501

Contents lists available at ScienceDirect

Physics Letters B

www.elsevier.com/locate/physletb

Tetrahedral symmetry in the ground state of ^{16}O

X.B. Wang [a,*], G.X. Dong [a], Z.C. Gao [b], Y.S. Chen [b], C.W. Shen [a]

[a] School of Science, Huzhou University, Huzhou 313000, China
[b] China institute of atomic energy, Beijing 102413, China

ARTICLE INFO

Article history:
Received 13 December 2018
Received in revised form 31 January 2019
Accepted 1 February 2019
Available online 6 February 2019
Editor: W. Haxton

Keywords:
Tetrahedral symmetry
Cluster-like structure

ABSTRACT

Based on the Skyrme energy density functional, the self-consistent HF calculations have been performed for ^{16}O, and the results show that the double point group tetrahedral symmetry T_d^D may play an important role in the configuration of many-body fermion system in the ground state of ^{16}O. The corresponding total density distribution in the ground state, calculated by using the HF wave functions, presents the distinct 4α cluster-like tetrahedral structure with the T_d symmetry. Among others, the necessary restoration of the rotational and parity symmetry, plays a crucial role for the occurrence of the tetrahedral symmetry in ^{16}O.

The tetrahedral symmetry that breaks spontaneously both the spherical and spatial-reflection symmetries has been identified in molecules, fullerenes, metal clusters and many other quantum objects, all of which are governed by electromagnetic interaction. A matter of fundamental interest has been the possibility of the tetrahedral symmetry in atomic nuclei, as a strong interaction finite many-body quantum system. Recently, the low-lying tetrahedral states were predicted by the potential energy surface calculations to appear in ^{156}Gd [1]. To test the tetrahedral symmetry the ultrahigh-resolution gamma-ray spectroscopy of ^{156}Gd was carried out in a collaboration between France, Poland, Bulgaria, Switzerland and Italy [2]. The experimental result, however, gives a strong evidence against tetrahedral symmetry in the lowest negative-parity band of ^{156}Gd. The same conclusion for the non-tetrahedral symmetry of this negative-parity band also was drawn by another experimental data [3]. The searching for new candidates for the tetrahedral symmetry in other nuclear mass regions becomes an important task to address the issue.

Very recently, the evidence for the tetrahedral symmetry in light nucleus ^{16}O has been identified by Bijker and Iachello with the algebraic cluster model to reproduce the rotation-vibration spectrum of an object with T_d symmetry (tetrahedral) and compare it with the observed ground state rotational band in ^{16}O [4]. This study clearly shows that the low-lying states in ^{16}O can be described as a 4α cluster with T_d symmetry for both the energies and the $B(EL)$ values of the ground-band states. A very recent *ab initio* lattice calculation of the low-lying even-parity states of ^{16}O has been carried out in the framework of nuclear lattice effective field theory, and the result also shows that the nucleons in the ground state of ^{16}O are arranged in a tetrahedral configuration of 4α clusters [5]. The fingerprints of tetrahedral configuration in ^{16}O is also found from the investigation of giant dipole resonance [6].

In this letter, we report our investigation based on the nuclear mean-field solution for the tetrahedral symmetry in the ground state of ^{16}O rather than the starting point of the α-cluster picture. The specific results may, therefore, provide a deeper insight into the tetrahedral symmetry in the nuclear system where the mean field approximation has been proven as an essential starting point for the nuclear modelings. We will show that the HF calculation based on the Skyrme energy density functional predicts the tetrahedral shape with double point group symmetry T_d^D as the major configuration in the ground state of ^{16}O, and the beyond mean-field effect, namely, the restoration of rotational symmetry, plays a crucial role in the occurrence of the tetrahedral symmetry. We show also that the ground state of ^{16}O with the tetrahedral T_d^D symmetry has a density distribution of nuclear matter presenting a 4α-cluster structure with the T_d symmetry.

The density functional theory (DFT) is based on theorems presenting the existence of energy functionals for many-body systems, which, in principle, include all many-body correlations [7–9]. Actually, the first nuclear energy density functionals have been presented in the context of the Hartree–Fock (HF) method with the zero range, density dependent interactions such as the Skyrme force [10–12]. The potential energy surfaces (PES) is obtained by the constraints of multipole moments $\bar{Q}_{\lambda\mu}$, using the augmented Lagrangian method, which is very robust and can give precisely the

* Corresponding author.
E-mail address: xbwang@zjhu.edu.cn (X.B. Wang).

https://doi.org/10.1016/j.physletb.2019.02.001

requested solutions [13]. During PES calculations, a constraint is always imposed on the center of mass of the nucleus: $\langle r^1 Y_{10}\rangle = 0$, to exclude the possible coupling to the spurious center of mass motion.

The symmetry restoration is very important to study the "true" ground and excited states of deformed nuclei, for references of investigating tetrahedral symmetry, see Refs. [14–16]. In the deformed mean field, the angular-momentum-projection (AMP) operator $\hat{P}^I_{MK}$ and parity projection operator $\hat{P}^\pi$ [17,18], can be used to obtain the angular momentum and parity conserving wave function,

$$|IMK^\pi\rangle = \hat{P}^I_{MK}\hat{P}^\pi|\Phi\rangle \equiv \frac{2I+1}{8\pi^2}\int D^{I*}_{MK}(\Omega)\,\hat{R}(\Omega)|\Phi^\pi\rangle\,d\Omega, \qquad (1)$$

where, I is the angular momentum, and M and K are its projections along the laboratory and intrinsic z axes, respectively. $\hat{P}^\pi = 1/2(1+\pi\hat{P})$, where $\hat{P}$ is the parity operator and $\pi = \pm 1$. Ω denotes the set of three Euler angles (α, β, γ), while $D^{I*}_{MK}(\Omega)$ are Wigner functions [19]. $\hat{R}(\Omega) = e^{-i\alpha\hat{I}_z}e^{-i\beta\hat{I}_y}e^{-i\gamma\hat{I}_z}$ is the rotation operator.

As the rotation symmetry is broken in the mean field, K is no longer a good quantum number, so that different K components must be mixed with the coefficients determined by minimizing the energy. The K-mixing is realized by the assumption,

$$|IM^\pi\rangle^{(i)} = \sum_K g^{(i)}_K |IMK^\pi\rangle \equiv \sum_K g^{(i)}_K \hat{P}^I_{MK}|\Phi^\pi\rangle, \qquad (2)$$

where $g^{(i)}_K$ are the mixing coefficients of different K components. The label $i = 1, 2, \ldots$ indicates the different collective states with the same angular momentum I. Then the Hill–Wheeler (HW) [20] equation is solved to obtain the eigen energies $E^{I^\pi}_i$ and mixing coefficients $g^{(i)}_K$,

$$\mathcal{H}^{I^\pi}\bar{g}^{(i)} = E^{I^\pi}_i \mathcal{N}^{I^\pi}\bar{g}^{(i)}, \qquad (3)$$

where the matrix elements $\mathcal{H}^{I^\pi}_{K'K} = \langle\Phi|\hat{H}\hat{P}^I_{K'K}\hat{P}^\pi|\Phi\rangle$ and $\mathcal{N}^I_{K'K} = \langle\Phi|\hat{P}^I_{K'K}\hat{P}^\pi|\Phi\rangle$ represent the Hamiltonian and overlap kernels, respectively. $\bar{g}^{(i)}$ represents a column of the $g^{(i)}_K$ coefficients. States with different angular momentum and parity I^π are solved separately. When solving Eq. (3), the norm matrix is diagonalized to build the collective subspace. To avoid the numerical unstable solution, the cut-off parameter needs to be used to remove the "zero" norm eigenstates. The cut-off is chosen to satisfy the plateau condition for the corresponding state [21].

The EDF calculation and its extensions in this work are performed by the computer code HFODD (v2.73y) [22], which can solve HF/HFB equations in the basis of three-dimensional Cartesian harmonic oscillators. The AMP is provided by the code HFODD already and we implemented the parity projection for the current study. Calculations were performed in the spherical basis of 12 major harmonic-oscillator shells. The harmonic oscillator frequency of the basis is chosen as 1.2×41 MeV/A (the value 1.2 is based on experience of diagonalizing the Woods–Saxon Hamiltonian on the HO basis [23,24]). During the calculations, we break all intrinsic symmetries of the nuclear mean field, *i.e.*, simplex, signature, and parity symmetry, to adopt all possible deformation freedoms. The AMP energy and overlap kernels are calculated by using 40 Gauss–Chebyshev integration points in the α and γ directions and 40 Gauss–Legendre points in the β direction.

We use several Skyrme-EDFs, as the SLy4 [25], SIII [26], and SkP [27] functionals which are frequently used for DFT predictions, to initiate the calculations. The SkV [26] functional, derived from the density-independent force and free from singularity problem existed in multi-reference calculations [28,29], also serves DFT predictions commonly, especially for beyond-mean-field descriptions [30,31].

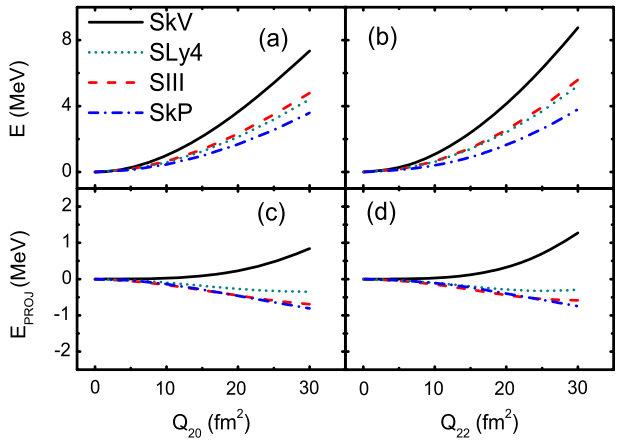

Fig. 1. Mean-field energy E, projected energy $E_{\rm PROJ} = E^{I=0}_1$ in function of the quadrupole moments $\hat{Q}_{20}$ (left) and $\hat{Q}_{22}$ (right), calculated for ^{16}O by the SkV, SLY4, SIII, and SKP functionals.

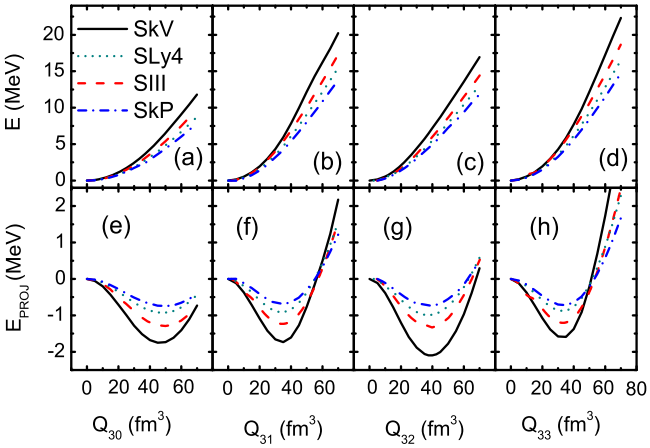

Fig. 2. Same as Fig. 1, but for octupole moments $\hat{Q}_{30}$, $\hat{Q}_{31}$, $\hat{Q}_{32}$ and $\hat{Q}_{33}$. The quadrupole moments are set to zero during these calculations.

We first calculate the energy curves against one deformation freedom only, while other deformations are forced to be zero. The results for quadrupole deformations and octupole deformation, are shown in Figs. 1 and 2, respectively. The mean field energies from variational calculations are shown in the upper panel of the figures. The lowest projected energies $E^{I=0}_1$, in function of the quadrupole moments (Fig. 1) and octupole moments (Fig. 2), are shown in the lower panel, labeled as $E_{\rm PROJ}$. As expected, in the mean-field energy curves of ^{16}O there is a deep minimum at the spherical configuration and no other local minimum. The projected energy curves are extremely flat against quadrupole deformations, being consistent with the results in Ref. [32].

However, when the necessary restoration of the rotational symmetry is considered through the angular momentum plus parity projection (AMPP), the octupole deformed states become lower in energy than the spherical state, as the well established minima seen in the lower panel of Fig. 2. For all these Skyrme functionals, non-axial octupole minima with moment $\hat{Q}_{32}$ are slightly lower than axial deformed one with $\hat{Q}_{30}$, and are also slightly lower than the corresponding other non-axial octupole minima. Especially, the results from the SkV functional shows that the $\hat{Q}_{32}$-deformed min-

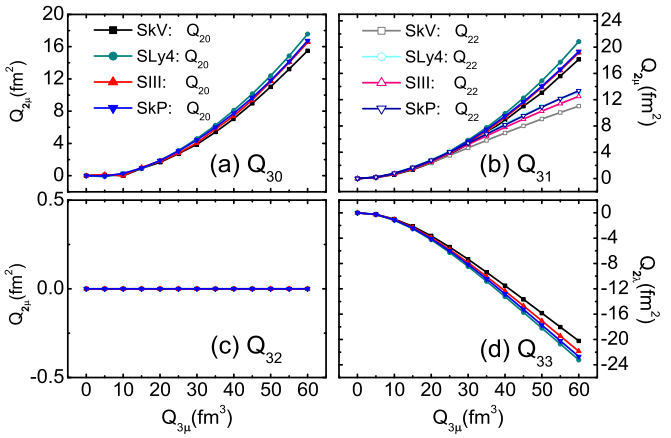

Fig. 3. The quadrupole moments against the octupole moments, during the HF variations for the calculation with constraints of octupole moments.

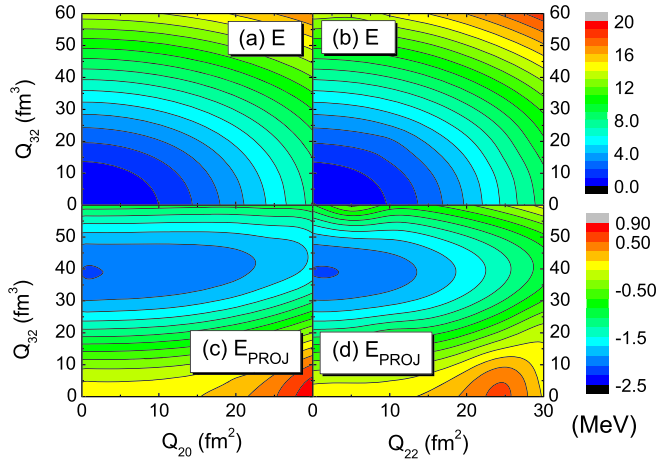

Fig. 4. Potential energy surfaces in the $(\hat{Q}_{20}, \hat{Q}_{32})$ (left) and $(\hat{Q}_{22}, \hat{Q}_{32})$ (right) plane, calculated by SkV functionals. The contour scale is 1.0 MeV for the mean-field energy E (a) and (b), and 0.2 MeV for the projected energy E_{PROJ} (c) and (d).

imum is explicitly lowest. In general, the HF solutions with the Skyrme functionals and AMPP indicates that the system in the ground state of ^{16}O favors to have the Y_{32} shape, the tetrahedral symmetry.

We also do the variations against single octupole deformation without constraints of other deformation freedom. The unconstrained moments, e.g., quadrupole and other octupole moments are initialized as zero. Thus, they can occur naturally during the HF variations (minimizing procedure). The quadrupole moments after convergence are shown in Fig. 3. The other, unconstrained, octupole moments are nearly zero (less than 10^{-1} fm^3) after the convergence. As in Fig. 3 (a), when Q_{30} moment increases, Q_{20} moment grows, without triaxial deformations. When Q_{31} moment increases, Q_{20} moment increases and triaxality kicks in (Q_{22} moment appears), seen in Fig. 3 (b). As in Fig. 3 (c), when Q_{32} moment increases, no quadrupole deformation appears at all. The results of Q_{33} are similar as Q_{30} moment, as in the panel (d) of Fig. 3.

We then test the competition of the tetrahedral degree of freedom with the quadrupole and other octupole degrees of freedom. The potential energy surfaces in the $(\hat{Q}_{20}, \hat{Q}_{32})$ and $(\hat{Q}_{22}, \hat{Q}_{32})$ plane are given, calculated by using the SkV functionals and setting other multipole moments to zero during the entire computation, in Fig. 4. The Fig. 5 shows the energy surfaces in the $(\hat{Q}_{30}, \hat{Q}_{32})$, $(\hat{Q}_{31}, \hat{Q}_{32})$, and $(\hat{Q}_{33}, \hat{Q}_{32})$ plane, calculated with other multipole

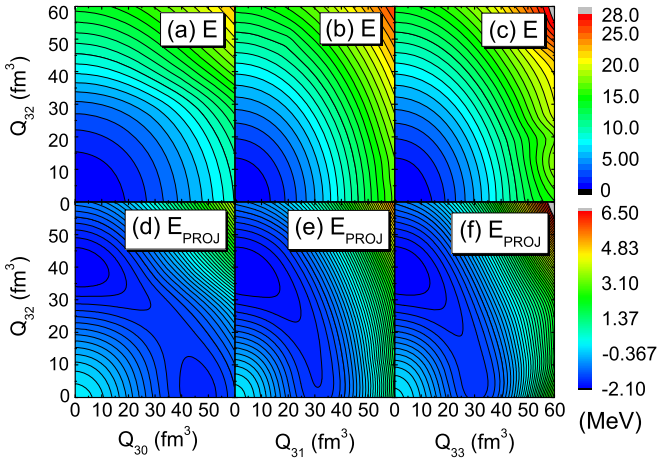

Fig. 5. Same as Fig. 4, but for energy surfaces in the $(\hat{Q}_{30}, \hat{Q}_{32})$, $(\hat{Q}_{31}, \hat{Q}_{32})$, and $(\hat{Q}_{33}, \hat{Q}_{32})$ plane. The contour scale is 1.0 MeV for the mean-field energy E (a), (b) and (c), and 0.15 MeV for the angular-momentum projected energy E_{PROJ} (d), (e) and (f).

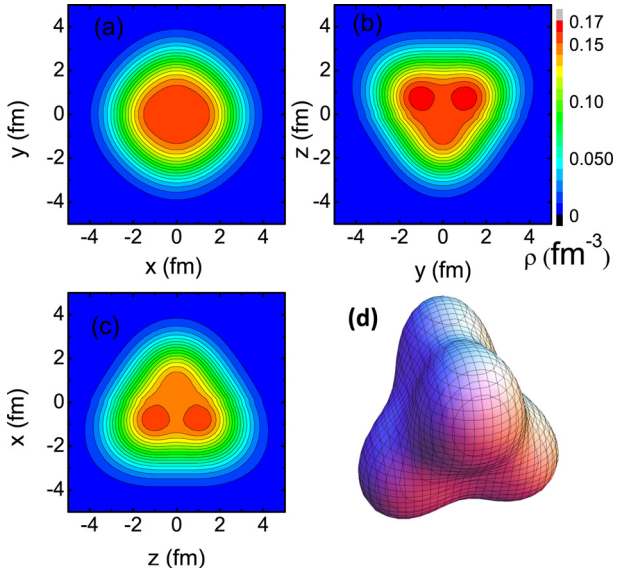

Fig. 6. (a–c) Density distributions of ^{16}O, with the pure moment $\hat{Q}_{32} = 40$ fm^3 ($\beta_{32} = 0.339$), calculated by SkV functional, in (x, y), (y, z), (z, x) planes, respectively. The contour scale is 0.01 fm^{-3}, and the third axis left, *i.e.*, z, x, y is fixed at 0.161 fm. (d) The 3D-density distribution of ^{16}O at the density $\rho = 0.15$ fm^{-3}.

moments being excluded. As expected, in the mean-field energy surfaces only the spherical minimum survives. After the restoration of the symmetry, the projected energy surfaces in the lower panel of Figs. 4 and 5, gives a pure $\hat{Q}_{32}$-deformed minimum, indicating the tetrahedral symmetry nature in the ground state of ^{16}O. The projected energies give rise to the tetrahedral minimum at about $Q_{32} = 40$ fm^3. The above projected energy surface calculations demonstrate that the tetrahedral degree of freedom as the non-axial octupole deformation, Y_{32}, could win against or strongly compete with the other important nuclear deformation degrees of freedom, namely, the quadrupole and other octupole deformations.

The total density distribution in the ground state of ^{16}O is calculated by using the wave function predicted by the projected energy surface of SkV functional, namely, with the tetrahedral shape at the moment $Q_{32} = 40$ fm^3 (tetrahedral minimum of the projected energy surfaces, as can be seen in Figs. 2, 4, and 5), and the results are plotted in Fig. 6. This total density distribution of ^{16}O, as a nucleonic system, coincides with the 4α-cluster structure

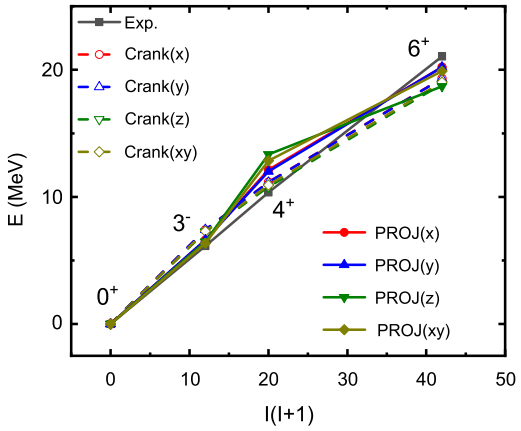

Fig. 7. The experimental ground-state band of ^{16}O, taken from the observed spectrum [34] and organized by Ref. [4], is given for a comparison with calculations (labeled as "Exp."). Calculated ground-state band of ^{16}O from the cranking-HF solution of tetrahedral symmetry with $Q_{32} = 40$ fm^3 with cranking axis as x, y, z and the axis in $x-y$ plane ($\pi/4$ degree between x and y axis), are labeled as "Crank(x)", "Crank(y)", "Crank(z)" and "Crank(xy)" respectively. The projection energies after the convergence of CHF with different cranking axis are also given (labeled as "PROJ(x)", "PROJ(y)", "PROJ(z)", and "PROJ(xy)" correspondingly).

of ^{16}O. Hence, the present Skyrme functional calculations could provide the microscopic support to the 4α-cluster modelings of the tetrahedral structure of ^{16}O, for an example, as that given in Ref. [4].

The tetrahedral rotational band is a very important proof for the tetrahedral symmetry [33]. In Ref. [4], the ground tetrahedral rotational band of ^{16}O has been used as the experimental indicator of tetrahedral symmetry. However, unlike the axially deformed nuclei, the favored cranking axis of the tetrahedral deformed state has uncertainties [35,36]. In principle, the tilted axis cranking needs to be performed. To test the collective rotation on the tetrahedral deformed state, we select several different cranking axis, as x axis, y axis, z axis, and the axis in xy plane ($\pi/4$ degree between x and y axis). We do the cranking calculation with the constraints of $\langle \hat{I} \rangle = I$ based on the tetrahedral-deformed minimum suggested by projected energy surface, by the SkV functional. The AMPP calculations is performed after the convergence of cranking-HF (CHF) calculations. In the CHF calculation, the time-odd field is also included. The projection after the convergence of cranking mean field can improve the description of the cranking momentum of inertia at low spins for projection calculations, which is an approximated variational-after-projection (VAP) method [21,37]. Results are shown in Fig. 7. The total Routhians by different cranking axis at the same spin are quite close. Both the CHF and projection calculations can give good reproduction of the experimental tetrahedral rotational band of ^{16}O.

The present Skyrme functional HF calculations, as the microscopic mean-field study, could support, therefore, the conclusion that the tetrahedral symmetry as the 4α structure exists in the ground state of ^{16}O from the very recent studies, the algebraic cluster model (ACM) calculation [4] and the *ab initio* lattice calculation [5]. The necessary restoration of the rotational symmetry is essential for the appearance of well established tetrahedral minima in the projected energy surfaces generated by the Skyrme functionals. The spectrum calculations performed with the AMPP on the CHF solutions indicate again that the tetrahedral symmetry configuration might be a major one in the ground state of ^{16}O. As a typical quantum system, the "true" ground state ^{16}O should be a mixing of different possible configurations, and what matters most would be the relative importances for these configurations, so that, the mixing between different configurations, *i.e.*, spherical shape, quadrupole deformed shape, $Y_{32} - 4\alpha$, $^{12}C + \alpha$ structure, *etc.*, have to be performed in the future, to understand the full picture of the ground state in ^{16}O.

Acknowledgements

This work has been supported by the National Natural Science Foundation of China under Grant Nos. U1732138, 11505056, 11605054, 11575290, 11490560, 11847315, and 11790325.

References

[1] J. Dudek, D. Curien, N. Dubray, J. Dobaczewski, V. Pangon, P. Olbratowski, N. Schunck, Phys. Rev. Lett. 97 (2006) 072501.
[2] M. Jentschel, et al., Phys. Rev. Lett. 104 (2010) 222502.
[3] R.A. Bark, et al., Phys. Rev. Lett. 104 (2010) 022501.
[4] R. Bijker, F. Iachello, Phys. Rev. Lett. 112 (2014) 152501.
[5] E. Epelbaum, H. Krebs, T.A. Lähde, D. Lee, Ulf-G. Meißner, G. Rupak, Phys. Rev. Lett. 112 (2014) 102501.
[6] W.B. He, Y.G. Ma, X.G. Cao, X.Z. Cai, G.Q. Zhang, Phys. Rev. Lett. 113 (2014) 032506.
[7] P. Hohenberg, W. Kohn, Phys. Rev. 136 (1964) B864.
[8] M. Levy, Proc. Natl. Acad. Sci. USA 76 (1979) 6062.
[9] W. Kohn, L.J. Sham, Phys. Rev. 140 (1965) A1133.
[10] D. Vautherin, D.M. Brink, Phys. Rev. C 5 (1972) 626.
[11] J.W. Negele, Phys. Rev. C 1 (1970) 1260.
[12] J.W. Negele, D. Vautherin, Phys. Rev. C 5 (1972) 1472.
[13] A. Staszczak, M. Stoitsov, A. Baran, W. Nazarewicz, Eur. Phys. J. A 46 (2010) 85.
[14] K. Zberecki, P. Magierski, P.-H. Heenen, N. Schunck, Phys. Rev. C 74 (2006) 051302(R).
[15] K. Zberecki, P.-H. Heenen, P. Magierski, Phys. Rev. C 79 (2009) 014319.
[16] S. Tagami, Y.R. Shimizu, J. Dudek, Phys. Rev. C 87 (2013) 054306.
[17] R.E. Peierls, J. Yoccoz, Proc. Phys. Soc. Lond. A 70 (1957) 381.
[18] P. Ring, P. Schuck, The Nuclear Many-Body Problem, Springer-Verlag, Berlin, 1980.
[19] D.A. Varshalovich, A.N. Moskalev, V.K. Khersonskii, Quantum Theory of Angular Momentum, World Scientific, Singapore, 1988.
[20] D.L. Hill, J.A. Wheeler, Phys. Rev. 89 (1953) 1102.
[21] H. Zdunczuk, J. Dobaczewski, W. Satuła, Int. J. Mod. Phys. E 16 (2007) 377.
[22] N. Schunck, J. Dobaczewski, J. McDonnell, W. Satuła, P. Bączyk, J. Dudek, Y. Gao, M. Konieczka, K. Sato, Y. Shi, X.B. Wang, T.R. Werner, Comput. Phys. Commun. 216 (2017) 145.
[23] J. Dudek, Z. Szymańfiski, T.R. Werner, Phys. Rev. C 23 (1981) 920.
[24] S. Ćwiok, J. Dudek, W. Nazarewicz, J. Skalski, T. Wemer, Comput. Phys. Commun. 46 (1987) 379.
[25] E. Chabanat, P. Bonche, P. Haensel, J. Meyer, R. Schaeffer, Nucl. Phys. A 635 (1998) 231.
[26] M. Beiner, H. Flocard, N. Van Giai, P. Quentin, Nucl. Phys. A 238 (1975) 29.
[27] J. Dobaczewski, H. Flocard, J. Treiner, Nucl. Phys. A 422 (1984) 103.
[28] J. Dobaczewski, M.V. Stoitsov, W. Nazarewicz, P.-G. Reinhard, Phys. Rev. C 76 (2007) 054315.
[29] T. Duguet, M. Bender, K. Bennaceur, D. Lacroix, T. Lesinski, Phys. Rev. C 79 (2009) 044320.
[30] W. Satuła, J. Dobaczewski, W. Nazarewicz, M. Rafalski, Phys. Rev. Lett. 106 (2011) 132502.
[31] W. Satuła, et al., Phys. Rev. Lett. 103 (2009) 012502;
Phys. Rev. C 81 (2010) 054310.
[32] M. Bender, P.-H. Heenen, Nucl. Phys. A 713 (2003) 390.
[33] J. Dudek, D. Curien, I. Dedes, K. Mazurek, S. Tagami, Y.R. Shimizu, T. Bhattacharjee, Phys. Rev. C 97 (2018) 021302(R).
[34] D.R. Tilley, H.R. Weller, C.M. Cheves, Nucl. Phys. A 564 (1993) 1.
[35] N. Schunck, J. Dudek, S. Frauendorf, Acta Phys. Pol. B 36 (2005) 1071.
[36] N. Schunck, P. Olbratowski, J. Dudek, J. Dobaczewski, Int. J. Mod. Phys. E 15 (2006) 490.
[37] H. Zdunczuk, W. Satuła, J. Dobaczewski, M. Kosmulski, Phys. Rev. C 76 (2007) 044304.